Hypoxia-Inducible Factor-1 Target Genes as Indicators of Tumor Vessel Response to Vascular Endothelial Growth Factor Inhibition

Duyen T. Dang,[1,3] Sang Y. Chun,[2] Kyunghee Burkitt,[2] Masako Abe,[4] Shaowei Chen,[2] Pamela Havre,[4] Nicola J. Mabjeesh,[5] Elisabeth I. Heath,[6] Nicholas J. Vogelzang,[4] Marcia Cruz-Correa,[7] Douglas W. Blayney,[2,3] William D. Ensminger,[2,3] Brad St. Croix,[8] Nam H. Dang,[4] and Long H. Dang[2,3]

[1]Division of Gastroenterology, [2]Division of Hematology/Oncology, Department of Internal Medicine, The University of Michigan Medical Center, [3]University of Michigan Comprehensive Cancer Center, Ann Arbor, Michigan; [4]Nevada Cancer Institute, Las Vegas, Nevada; [5]Prostate Cancer Research Laboratory, Department of Urology, Tel Aviv Sourasky Medical Center, Tel Aviv, Israel; [6]Barbara Ann Karmanos Cancer Institute, Wayne State University, Detroit, Michigan; [7]The University of Puerto Rico Cancer Center, San Juan, Puerto Rico; and [8]National Cancer Institute, Frederick, Maryland

Abstract

Antiangiogenic therapy improves survival in patients with advanced stage cancers. Currently, there are no reliable predictors or markers for tumor vessel response to antiangiogenic therapy. To model effective antiangiogenic therapy, we disrupted the *VEGF* gene in three representative cancer cell lines. HCT116 xenografts had low proportions of endothelial tubes covered by pericytes that stained with α-smooth muscle actin (SMA) antibody. Upon disruption of *VEGF*, HCT116$^{VEGF-/-}$ xenografts had significantly decreased tumor microvessel perfusion compared with their parental counterparts. Furthermore, HCT116$^{VEGF-/-}$ xenografts mounted a tumor-reactive response to hypoxia, characterized by the induction of hypoxia-inducible factor-1 (HIF-1) target genes. One highly induced protein was DPP4, a measurable serum protein that has well-described roles in cancer progression. In contrast, LS174T and MKN45 tumor xenografts had high proportion of endothelial tubes that were covered by SMA+ pericytes. Upon disruption of VEGF, LS174T$^{VEGF-/-}$ and MKN45$^{VEGF-/-}$ xenografts maintained tumor microvessel perfusion. As such, there were no changes in intratumoral hypoxia or HIF-1α induction. Together, these data show that the extent of tumor vessel response to angiogenic inhibition could be correlated with (*a*) the preexisting coverage of tumor endothelial tubes with SMA+ pericytes and (*b*) differential tumor induction of HIF-1 target genes. The data further show that DPP4 is a novel marker of HIF-1 induction. Altogether, these preclinical findings suggest novel clinical trials for predicting and monitoring tumor vessel responses to antiangiogenic therapy. [Cancer Res 2008;68(6):1872–80]

Introduction

Vascular endothelial growth factor A (VEGFA or VEGF) is the most ubiquitous activator of tumor angiogenesis (1–3). In fact, the incorporation of agents targeting VEGF, or VEGF receptors, has been a major milestone in the treatment of cancer. In phase III clinical trials, the addition of humanized anti-VEGF monoclonal antibody, bevacizumab, to standard chemotherapy, led to increased response in patients with advanced colorectal, breast, and lung cancers (4–6). In phase III clinical trials, treatment with the multitargeted tyrosine kinase inhibitors sunitinib and sorafenib, which block VEGF receptor 2 along with other kinases, significantly improved time-to-progression in patients with gastrointestinal stromal tumors and renal cell cancer (7–9). There are currently no reliable predictors or markers of antiangiogenic response. A better understanding of the determinants, and consequences, of antiangiogenic response would have significant clinical implications.

Pericytes are mural cells that surround endothelial tubes. It is thought that pericytes stabilize tumor endothelial cells against anti-VEGF therapy. It is likely that the extent of tumor endothelial cells–pericytes (E–P) interaction is associated with the types of response to antiangiogenic therapy. As such, examination of E–P interactions in patients' tumors is currently under investigation, as a predictive marker for antiangiogenic response (10).

Levels of expression of hypoxia-inducible factor-1α (HIF-1α) and HIF-1 target genes (i.e., *CA IX, GLUT1*, and *LDH*) have been studied as prognostic markers in various cancer types (11–13). When antiangiogenic therapy causes tumor vessel regression, there is increased intratumoral hypoxia, stabilization of HIF-1α, and induction of HIF-1 target genes (14, 15). However, it remains unclear whether the induction of HIF-1 target genes can be used as markers for response to antiangiogenic therapy. In this report, we show that the extent of tumor microvessel response to VEGF inhibition correlates with the preexisting E–P interactions in the tumor vasculature, and can be distinguished by the tumor-reactive response to hypoxia.

Materials and Methods

Cell lines. All cancer cell lines were acquired from the American Type Culture Collection with the exception of MKN45. CAPAN-1 is a human pancreatic cancer cell line. HCT116, HT29, KM12L4, LOVO, LS174T, RKO, and SW480 are human colon cancer cell lines. HEP3B and SNU398 are human hepatocellular carcinoma cell lines. SIHA is a human cervical squamous cell carcinoma cell line. The MKN45 human gastric cancer cell line was acquired from the Japanese Collection of Research Bioresources/Human Science Research Resources Bank. Cells were cultured in the recommended medium, supplemented with 10% fetal bovine serum and 1% penicillin/streptomycin (Invitrogen). For normoxic culture conditions, cells were incubated at 37°C, in 5% CO_2 and room air (21% O_2). For hypoxic

Note: Supplementary data for this article are available at Cancer Research Online (http://cancerres.aacrjournals.org/).

Requests for reprints: Long H. Dang, The University of Michigan Medical Center, 1150 West Medical Center Drive, MSRB I, 6514 Ann Arbor, MI 48109. Phone: 734-647-2964; Fax: 734-763-2535; E-mail: lhdang@umich.edu.

doi:10.1158/0008-5472.CAN-07-1589

culture conditions, cells were incubated at 37°C in a BBL GasPak 100 anaerobic system, in which O_2 was ~0.1% (BD Biosciences).

***In vivo* tumorigenesis.** Six-week-old female athymic *nu/nu* mice (Charles River Labs) were implanted s.c. into the flanks, with 10×10^6 cells, as previously described (16). Tumor sizes were measured in two dimensions with calipers, and volumes were calculated with the formula $(L \times W^2) \times 0.5$, where L is length and W is width. Student's paired t test was used to determine statistical significance between groups. Mice were housed in barrier environments, with food and water provided *ad libitum* as approved by the University of Michigan Animal Care and Use Committee. Xenografts were harvested for subsequent analyses when they reached ~0.4 cm^3.

Immunofluorescence. Harvested xenografts were fixed in Tissue-Tek OTC compound (Sakura Finetek) and stored at −80°C. Frozen sections, 10 μm in thickness, were prepared with a Leica Microsystems cryostat. For tumor microvessel density (MVD) determination, sections were sequentially incubated with a monoclonal antibody against the endothelial cell–specific marker CD31 (BD PharMingen), followed by a biotinylated secondary antibody (Jackson ImmunoResearch Laboratories), and rhodamine-streptavidin (Vector Labs). For double immunofluorescence staining, sections were incubated with primary antibodies which were raised in different species: rat anti-CD31 (BD PharMingen), rabbit anti-NG2 (Chemicon), or mouse anti-SMA (Sigma). After washes, species-specific secondary antibodies coupled to rhodamine or FITC were applied. The absence of cross-reactivity among secondary antibodies against primary antibodies was verified by omitting one primary antibody during the first incubation. At least three sections of each of three tumors, representing middle and distal parts of the tumor were examined under fluorescence microscopy, and representative results are illustrated in the figures.

Quantification of staining. Images were captured on SPOT software and analyzed with Image-Pro Plus software (Diagnostic Instruments). To determine MVD, the percentage of the image field that stained with CD31 antibodies was measured. To determine tumor blood flow, the percentage of the image field that stained with Hoechst 33342 was measured. To determine endothelial tube length, at least 20 CD31-staining endothelial tubes were traced and measured. To determine endothelial coverage by pericytes, images were superimposed, and the percentage of overlapping or adjacent staining were measured. All measurements were made in at least nine separate images and averaged.

Disruption of the human *VEGF* and *HIF-1α* genes. The endogenous locus, adeno-associated virus knockout construct, and resulting targeted locus are shown in Fig. 1*A*. The strategy has been previously described (17). Exon 2 of *VEGF* was targeted for disruption with an adeno-associated virus cassette containing the *Neo* resistance gene under the constitutive control of a *SV40* promoter flanked by left and right homology arms approximately 1 kb in length. Cells exhibiting neomycin resistance were screened with locus-specific PCR (Fig. 1*B*). Once the first allele was successfully targeted, the *Neo* resistance gene was excised using *Cre* recombinase. The same targeting vector was then used to target the second allele. Loss of VEGF was confirmed by ELISA (Fig. 1*C*). Disruption of HIF-1α, and its confirmation, has been previously described (16).

ELISA for VEGF. An equal number of cells were plated overnight. The VEGF protein level in cultured medium was analyzed using the Quantikine VEGF ELISA Kit (R&D Systems) following the manufacturer's protocol.

Assessment of tumor vessel perfusion. Mice bearing parental or *VEGF−/−* xenografts were i.v. injected with Hoechst 33342 (40 mg/kg), 2 min prior to sacrifice. Tumors were fixed in Tissue-Tek OTC compound and stored at −80°C. Frozen sections 10 μm in thickness were prepared with a Leica Microsystems cryostat and examined under fluorescence microscopy.

Assessment of intratumoral hypoxia. To examine intratumor hypoxia, mice were administered the hypoxia marker pimonidazole, 60 mg/kg i.p. 2 h before sacrifice. Pimonidazole binds to the thiol-containing proteins specifically in hypoxic cells (18). Intraperitoneal injection of pimonidazole results in its uptake by hypoxic tumor cells, and bound pimonidazole can be detected in xenografts using antibodies to pimonidazole (18).

Immunohistochemistry. Harvested xenografts were fixed in formalin, paraffin-embedded, sectioned, and stained with H&E by the University of Michigan Tissue Core Facility. Bound pimonidazole was detected using the Hypoxyprobe-1 Plus kit (Chemicon).

Gene expression profiling. $HCT116^{VEGF-/-}$ and $HCT116^{VEGF-/-HIF-1\alpha-/-}$ xenografts were harvested at ~0.4 cm^3 and total RNA was extracted. Gene expression analyses on the samples were performed at the University of Michigan Comprehensive Cancer Center Affymetrix Core Facility. Commercial high-density oligonucleotide arrays were used (GeneChip Human Genome U133A; Affymetrix, Inc.), following protocols and methods developed by the supplier.

Real-time reverse transcription-PCR analyses. Total RNA from cell lines or xenografts were extracted, treated with DNase I, and reverse-transcribed as previously described (16). Real-time PCR reactions were performed in triplicate on reverse transcription–derived cDNA, and relative values calculated as previously described (19).

Western blot analyses. Whole-cell protein extracts were prepared from cell lines or individual xenografts, separated by electrophoresis, transferred to nitrocellulose membranes, and probed with antibodies as described previously (16). Antibodies were obtained from BD Transduction laboratories (mouse anti-human HIF-1α), Sigma (α-tubulin), Calbiochem (DPP4), Pierce (peroxidase-conjugated anti-rabbit antibody), and Jackson ImmunoResearch Laboratories (peroxidase-conjugated anti-mouse antibody). Antibody dilutions were as recommended by the manufacturer.

Bevacizumab treatment. For bevacizumab treatment, implanted tumors were allowed to grow to 0.1 cm^3 in volume, and then mice were treated with bevacizumab at 100 μg i.p., twice a week, for 2 weeks.

Results

Heterogeneity of the tumor vasculature and coverage by pericytes. Twelve human cancer cell lines, representing five epithelial cancer types (colon, pancreatic, liver, gastric, and cervical cancers), were selected for analyses. Tumor xenografts were grown in athymic nude mice and harvested once they reached ~0.4 cm^3. To analyze the structure of the tumor vasculature, frozen sections were stained with anti-CD31 antibody, a marker specific for endothelial cells. We observed significant heterogeneity in MVD and endothelial tube length in the 12 different xenografts (Table 1). Some tumors displayed high MVD and long endothelial tubes, whereas others displayed low MVD and short endothelial tubes.

Pericytes are mural cells that are characterized by their distinctive shape and location surrounding endothelial tubes. Several lines of evidence have suggested that pericytes stabilize tumor endothelial cells against anti-VEGF therapy. First, pericytes have been shown to support endothelial cells by secreting paracrine signals such as VEGF and angiopoietin-1 (Ang-1), and by providing stabilizing adhesive interactions through integrins such as α4β1 and N-cadherin (20, 21). Second, several animal models have shown the importance of pericytes in maintaining vascular integrity. For example, mouse embryos lacking platelet-derived growth factor-β (*PDGF-β*), or its receptor *PDGFR-β, Ang-1*, or its receptor *Tie-2*, develop blood vessels that are deficient in pericytes, abnormally large, and leaky (20, 22–24). Third, VEGF withdrawal led to the selective loss of immature, pericyte-negative vessels (25, 26). However, when both endothelial cells and pericytes were targeted by inhibitors, there was loss of both immature and mature vessels (27).

We thus also determined the percentage of tumor vessels that were covered by pericytes. Tumor xenograft sections were double-stained with anti-CD31 antibody for endothelial cells, and anti-NG2 (high molecular weight melanoma-associated antigen) or anti-SMA (α-smooth muscle actin) antibodies for pericytes (20). We found that endothelial coverage with SMA-expressing pericytes ranged

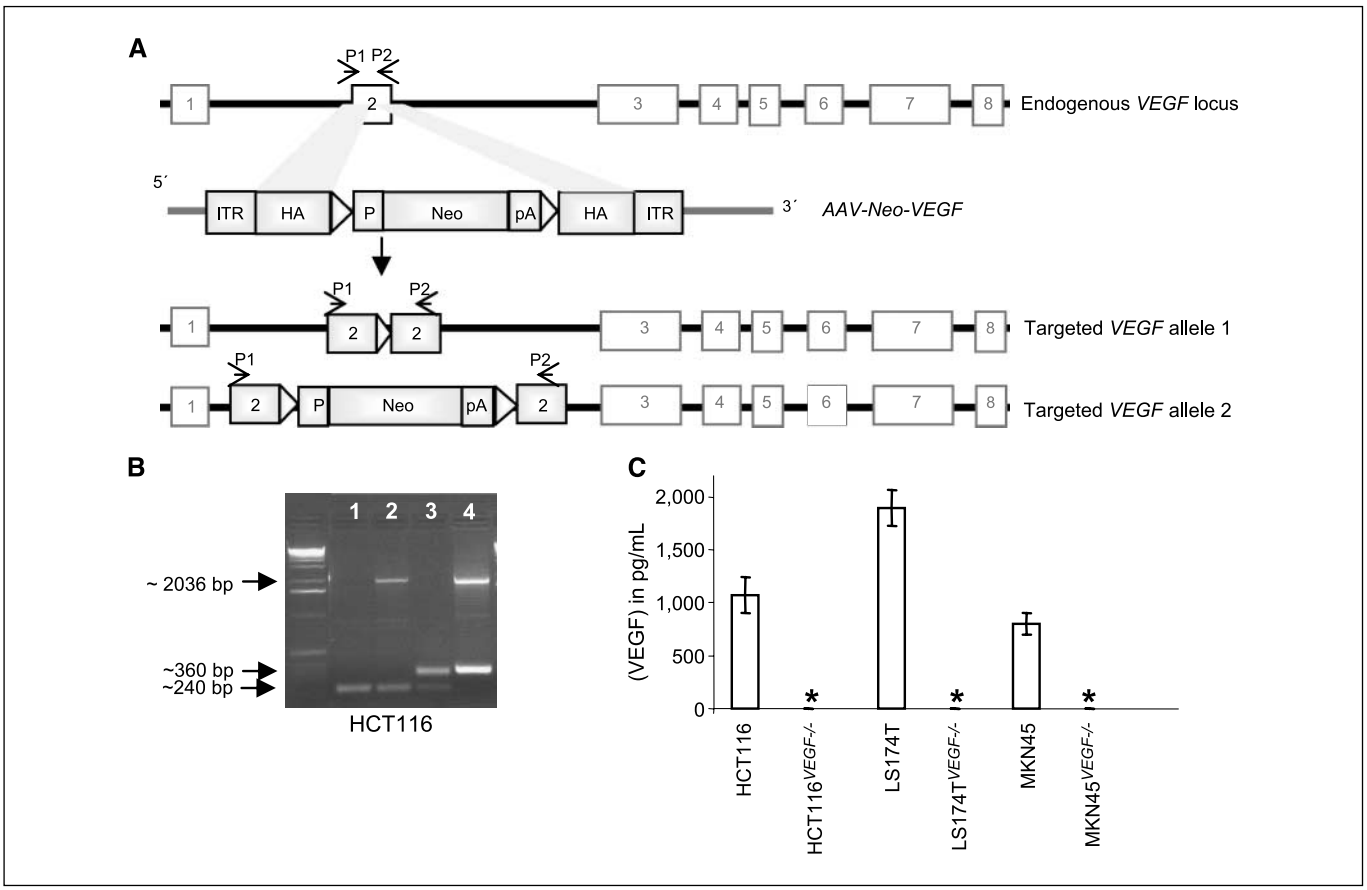

Figure 1. Disruption of *VEGF* in cancer cell lines. *A,* disruption of *VEGF*. The endogenous *VEGF* locus, adeno-associated virus knockout construct, and resulting targeted locus. *Numbered boxes,* exons. *Gray boxes,* targeted exon 2. *ITR,* inverted terminal repeats; *HA,* homology arm; *P,* SV40 promoter; *Neo,* neomycin resistance gene; *pA,* poly(A) tail; *arrowheads,* loxP sites; *P1/P2,* primers for locus-specific PCR. *B,* locus-specific PCR to confirm homologous integration of the targeting vector. PCR primers were designed to amplify only within the exon targeted for disruption (between arrows; see *P1* and *P2* in *A*). *Lane 1, VEGF+/+* cells: only the native loci (~240 bp) are amplified. *Lane 2, VEGF+/–* cells: the ~2036 bp product is the locus with targeting vector inserted, and the ~240 bp product is the native locus on the second allele. *Lane 3, VEGF+/–* cells: the ~360 bp product is the disrupted locus, with *Neo* removed by *Cre* recombinase. *Lane 4, VEGF–/–* cells: the ~2036 bp product is the second locus with the targeting vector inserted; the ~360 bp product is the disrupted locus on the first allele. *C,* ELISA for human VEGF.

from 28.6% to 90.5%, and endothelial coverage with NG2-expressing pericytes ranged from 39.3% to 97.7% (Table 1). In total, the data in Table 1 show that tumor xenografts display heterogeneity in their vasculature and interactions with pericytes.

VEGF withdrawal leads to different extents of vessel regression in tumors. To model effective antiangiogenic therapy, as well as control for potential differences in perfusion across various vessel types, we disrupted the *VEGF* gene by homologous

Table 1. MVD, endothelial tube length, and endothelial tube coverage by pericytes in 12 cancer xenografts

Cell line	MVD (%)	Tube length (μm)	Coverage by SMA-expressing pericytes (%)	Coverage by NG2-expressing pericytes (%)
CAPAN-1	7.33 ± 0.04	121.9 ± 34.1	49.0	72.7
HCT116	3.21 ± 0.03	120.9 ± 21.6	29.8	92.7
HEP3B	4.13 ± 0.038	112.4 ± 48.4	35.4	47.9
HT29	12.51 ± 0.07	55.0 ± 17.4	84.8	90.0
KM12L4	4.61 ± 0.07	130.7 ± 28.1	45.3	72.0
LOVO	4.76 ± 0.03	100.9 ± 27.1	70.5	76.5
LS174T	4.48 ± 0.04	158.6 ± 36.1	53.2	97.7
MKN45	2.40 ± 0.03	122.8 ± 34.5	53.4	75.8
RKO	1.10 ± 0.01	44.3 ± 19.8	90.5	69.8
SIHA	3.07 ± 0.01	80.1 ± 18.8	62.3	64.2
SNU398	10.27 ± 0.14	267.0 ± 99.1	62.0	64.4
SW480	2.10 ± 0.02	46.8 ± 11.4	28.6	39.3

recombination (Fig. 1). The human cancer cell lines HCT116, LS174T, and MKN45 were selected because they represent a variety of tumor vasculature (Table 1). Xenografts from these tumors had MVDs ranging from 2.40% to 4.48%. HCT116 xenografts had endothelial tubes that were not well covered by SMA+ pericytes (29.8%), but were well covered by NG2+ pericytes (92.7%). In contrast, LS174T and MKN45 xenografts had endothelial tubes that were ~50% covered by SMA+ pericytes, and different quantities of NG2+ pericytes (97.7% and 75.8%, respectively). We targeted exon 2 of the *VEGF* gene locus for disruption (Fig. 1*A*). Because exon 2 is upstream of all potential *VEGF* alternative splicing sites, no VEGF products were predicted to be translated. Disrupted genotypes and loss of the *VEGF* gene product were confirmed by locus-specific PCR and ELISA specific for VEGF protein, respectively (Fig. 1*B* and *C*).

To determine the effects of *VEGF* disruption on tumor growth, cells were implanted into athymic nude mice to form xenografts. The overlying skin in the subcutaneous xenograft model showed blanching for the *VEGF−/−* xenografts, consistent with decreased vascular permeability (Fig. 2*A*). Examination of tumor volumes revealed that HCT116$^{VEGF-/-}$ xenografts had a marked delay in tumor growth, in comparison with HCT116 parental controls (Fig. 2*B*). In contrast, smaller differences in growth delay were noted in the LS174T$^{VEGF-/-}$ and MKN45$^{VEGF-/-}$ xenografts, when compared with their respective parental controls (Fig. 2*B*).

To determine whether the differences in tumor xenografts growth delay were secondary to differences in the effects of *VEGF* disruption on tumor MVD, we stained tumor sections with the endothelial cell marker CD31 (Fig. 2*C*; Table 2). HCT116$^{VEGF-/-}$ xenografts had extensive decreases in MVD compared with their parental controls. In contrast, the extent of decrease in MVD was much less in LS174T$^{VEGF-/-}$ and MKN45$^{VEGF-/-}$ xenografts, compared with their parental controls (Fig. 2*C*; Table 2).

Table 2. MVD and tumor perfusion

Cell line	MVD (%)	Tumor perfusion (%)
HCT116	3.1 ± 0.6	6.9 ± 0.06
HCT116$^{VEGF-/-}$	0.2 ± 0.03	1.3 ± 0.04
LS174T	4.8 ± 0.4	13.4 ± 0.07
LS174T$^{VEGF-/-}$	3.5 ± 0.8	10.7 ± 0.05
MKN45	2.5 ± 0.6	5.9 ± 0.04
MKN45$^{VEGF-/-}$	1.9 ± 0.3	5.6 ± 0.05

To determine if the residual vessels were functional, we determined tumor perfusion by injecting Hoechst 33342 i.v. into nude mice bearing parental versus *VEGF−/−* tumors (Fig. 2*C*; Table 2). HCT116$^{VEGF-/-}$ xenografts had significantly decreased perfusion. In fact, most of the perfusion was seen at the tumor capsule, likely contributed by mouse stromal vasculature. In contrast, LS174T$^{VEGF-/-}$ and MKN45$^{VEGF-/-}$ xenografts maintained tumor perfusion compared with their parental counterparts. These studies showed that the functional tumor vasculature was disrupted in HCT116$^{VEGF-/-}$ xenografts, whereas it was preserved

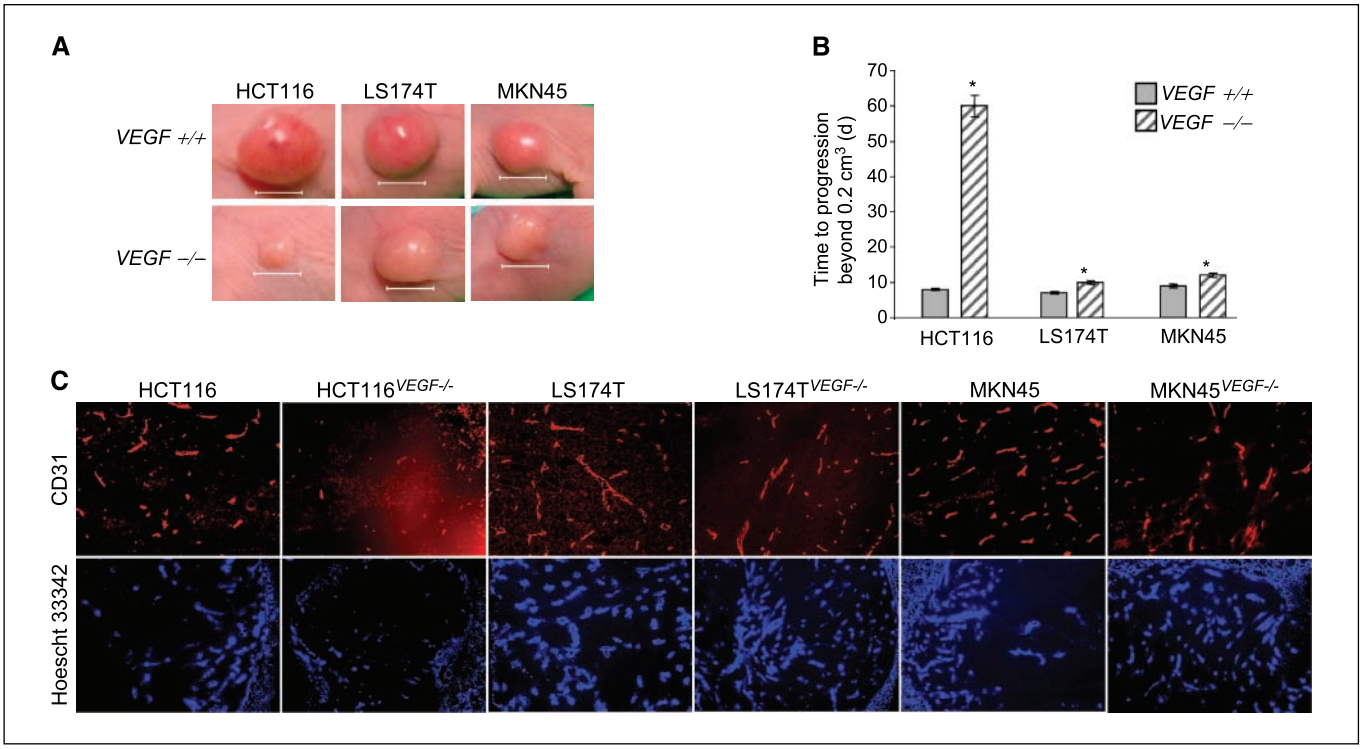

Figure 2. Tumor growth, MVD, and blood flow in *VEGF+/+* and *VEGF−/−* xenografts. *In vivo* xenograft growth assays were performed by implanting 10.0 × 10^6 tumor cells into the flanks of athymic nude mice and the ensuing xenograft growth was measured. *A,* examples of xenografts. *Bar,* 1.0 cm. *B,* time to tumor progression to 0.2 cm^3. Xenograft volumes were plotted as a function of time. The number of days for tumors to reach 0.2 cm^3 was calculated (n = 10 for each symbol). *, P < 0.01 comparing *VEGF−/−* to parental xenografts. *C,* tumor MVD and perfusion in parental and *VEGF−/−* xenografts. Endothelial cells were stained red with antibody to CD31 (*top row;* original magnification, ×100). Tumor perfusion is visualized as microvessels that had taken up Hoechst 33342 (*blue, bottom row;* original magnification, ×40).

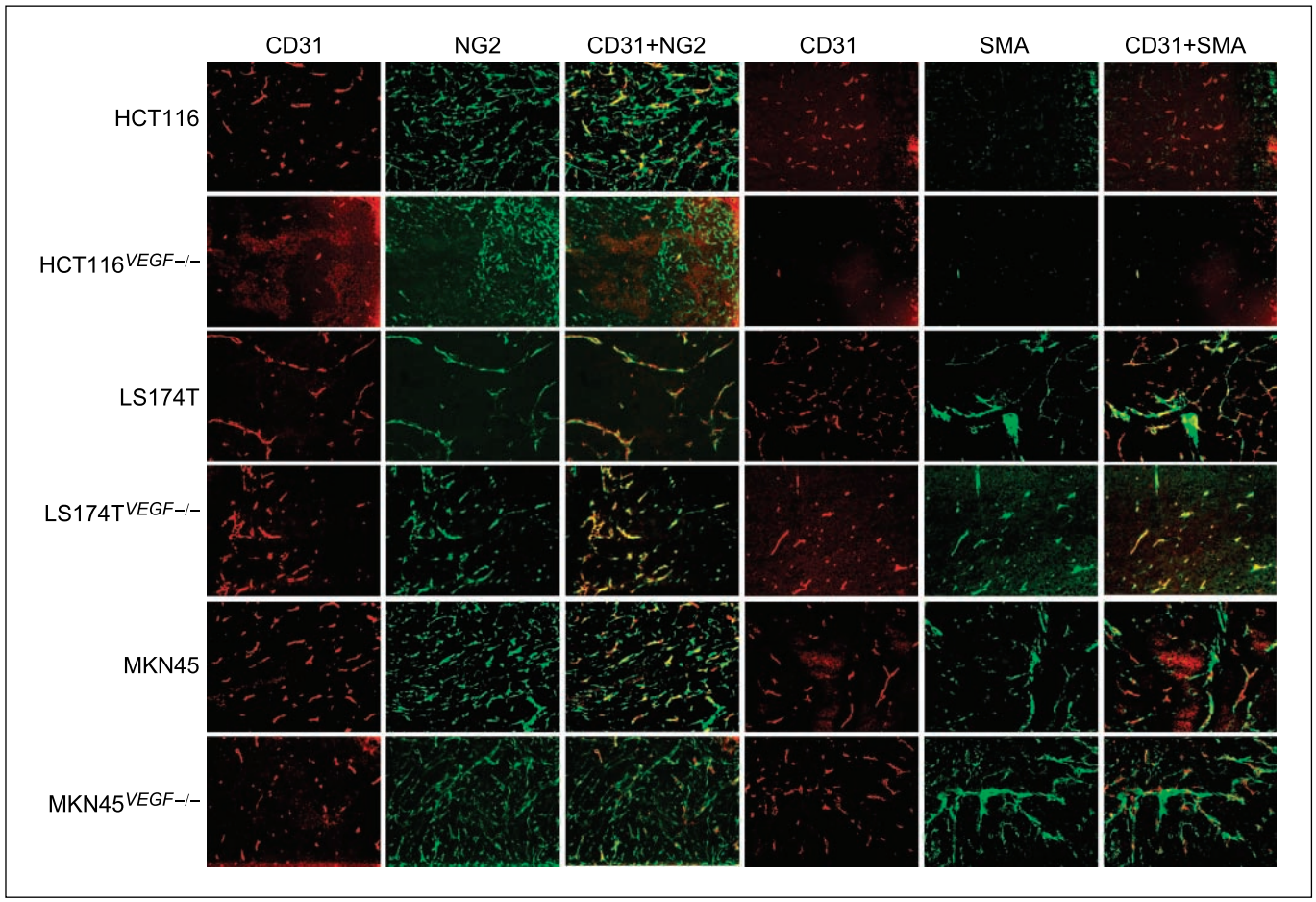

Figure 3. Vessel coverage by pericytes in *VEGF+/+* and *VEGF−/−* xenografts. To visualize endothelial cells and pericytes, xenograft sections were double-stained for endothelial cells and pericytes. Endothelial cells were detected with antibodies to CD31 (*red*). Pericytes were detected with antibodies to NG2 or SMA (*green*). Images were superimposed to show endothelial-pericyte association (either in *yellow* or *green*, immediately adjacent to *red*). Original magnification, ×100.

in LS174T$^{VEGF-/-}$ and MKN45$^{VEGF-/-}$ xenografts. As such, by analyzing these xenografts, we could gain insights into indicators of the extent of antiangiogenic response.

Because our model system employed HCT116 cells in which VEGF has been ablated, the decrease in MVD could be due to either vessel regression or decreased vessel formation. To address this question, we treated HCT116 xenografts with the anti-VEGF antibody bevacizumab (Supplementary Fig. S1). Treatment of HCT116 xenografts with bevacizumab led to significant tumor vessel regression and decreased tumor blood flow. This vessel regression phenotype is recapitulated in the HCT116$^{VEGF-/-}$ xenografts (Fig. 2*C*). As such, the decrease in MVD in this VEGF knockout model is most consistent with a vessel regression phenotype.

Vascular determinants associated with the extent of antiangiogenic response. Because E–P interactions are thought to affect tumor vessel response to VEGF inhibition, we analyzed E–P interactions in the various parental and *VEGF−/−* xenografts (Fig. 3). Endothelial cells were stained with anti-CD31 antibody, and pericytes with anti-NG2 or anti-SMA antibodies. We noted that the abundance of SMA-staining pericytes was correlated with the abundance of CD31-staining vessels in the *VEGF−/−* xenografts (Fig. 3). For example, LS174T$^{VEGF-/-}$ and MKN45$^{VEGF-/-}$ xenografts had more abundant SMA-staining pericytes, and higher associated residual endothelial tubes, than HCT116$^{VEGF-/-}$ xenografts. Going back to the parental xenografts, we noted that LS174T and MKN45 xenografts had ~50% of their endothelial tubes covered by SMA+ pericytes, whereas HCT116 had only ~29% coverage (Table 1). Thus, tumors with vessels that have enhanced coverage by SMA+ pericytes, for example LS174T and MKN45 xenografts, had maintained MVD in response to VEGF withdrawal (Table 2; Fig. 3). In contrast, tumors with lower vessel coverage by SMA+ pericytes, for example HCT116 xenografts, underwent significant vessel drop-out in response to VEGF withdrawal. It is possible that the quantity of SMA-staining pericytes indicates the density of well-protected endothelial tubes in a tumor, which in turn, would continue to be maintained after the disruption of *VEGF*. As such, the quantity of SMA-staining pericytes might predict tumor vessel response to antiangiogenic therapy.

In contrast, we observed that endothelial coverage by NG2-staining pericytes did not correlate with tumor vessel response. For example, HCT116 xenografts harbored abundant NG2-staining pericytes, but nonetheless, HCT116$^{VEGF-/-}$ xenografts had extensive tumor vessel regression (Fig. 3). In the same vein, HCT116$^{VEGF-/-}$ xenografts harbored abundant NG2-staining pericytes, which were minimally associated with the few remaining endothelial tubes (Fig. 3).

Previous studies have found that both SMA-staining and NG2-staining pericytes interact with endothelial cells in tumors (28, 29).

However, some tumors contain larger proportion of pericytes expressing NG2 than SMA, with subpopulations that were NG2-positive/SMA-positive and NG2-positive/SMA-negative (28, 29). Our data confirm previous findings that SMA-staining pericytes protect endothelial cells (25, 26). However, these are the first data to distinguish that SMA-staining pericytes, but not NG2-staining pericytes, are associated with vessel protection against VEGF withdrawal.

Disruption of VEGF increases intratumoral hypoxia, stabilizes HIF-1α, and induces HIF-1 target genes in tumors with extensive vessel response. We next asked whether the extent of antiangiogenic response is associated with changes in intratumoral hypoxia. Intratumoral hypoxia was determined by tumor uptake of the hypoxia marker pimonidazole (Fig. 4*A*). HCT116$^{VEGF-/-}$ xenografts, which were characterized by decreased MVD and poor perfusion, exhibited marked expansion of the tumor hypoxic compartments when compared with parental xenografts. On the other hand, LS174T$^{VEGF-/-}$ and MKN45$^{VEGF-/-}$ xenografts, which were characterized by preserved MVD and maintained perfusion, had no noticeable changes in intratumoral hypoxia when compared with their respective parental xenografts.

Tumor hypoxia leads to a reactive response in the tumor epithelial cells. This response is dominated by the induction of the transcription factor, HIF-1α, which is strongly associated with cancer cell growth and survival (11, 30–32). HIF-1 is composed of the HIF-1α and HIF-1β subunits. Whereas HIF-1β is constitutively expressed, HIF-1α protein stability and synthesis are regulated by intratumoral hypoxia and genetic alterations (11, 30–32). The HIF-1 complex directly transactivates more than 60 target genes, including those important for two universal characteristics of solid tumors: angiogenesis and glycolysis (11, 30–32). Thus, we next determined HIF-1α expression in the parental and *VEGF−/−* xenografts (Fig. 4*B*). Compared with parental xenografts, HCT116$^{VEGF-/-}$ had ~10-fold increased expression of HIF-1α. Conversely, there were no changes in HIF-1α expression in LS174T$^{VEGF-/-}$ and MKN45$^{VEGF-/-}$ xenografts compared with their respective parental xenografts. We proceeded to test the expression of four known HIF-1 target genes: aldolase A (*ALDOA*), glucose transporter 1 (*GLUT1*), lactate dehydrogenase A (*LDHA*), and phosphofructokinase, liver (*PFKL*). As shown in Fig. 4*D*, there was a significant ~1.3-fold to 2.3-fold increase in the expression of all four HIF-1 target genes in the HCT116$^{VEGF-/-}$ xenografts in comparison with the parental HCT116 xenografts. The induction of all four genes was HIF-1–dependent, as disruption of HIF-1α in the HCT116$^{VEGF-/-}$ xenografts reversed the induction of these genes (HCT116$^{VEGF-/-HIF-1\alpha-/-}$ versus HCT116 $^{VEGF-/-}$ xenografts; Fig. 4*D*). In contrast, LS174T$^{VEGF-/-}$ and MKN45$^{VEGF-/-}$ xenografts, compared with their respective parental xenografts, had no statistically significant changes in the expression of all four HIF-1 target genes (Fig. 4*D*). These data showed that the induction of HIF-1 target genes might be indicators of extensive vessel response and decreased tumor perfusion in response to antiangiogenic therapy. Conversely, the lack of induction of HIF-1 target genes might be indicators of lack of response, maintenance of tumor blood vessels, and continued tumor perfusion.

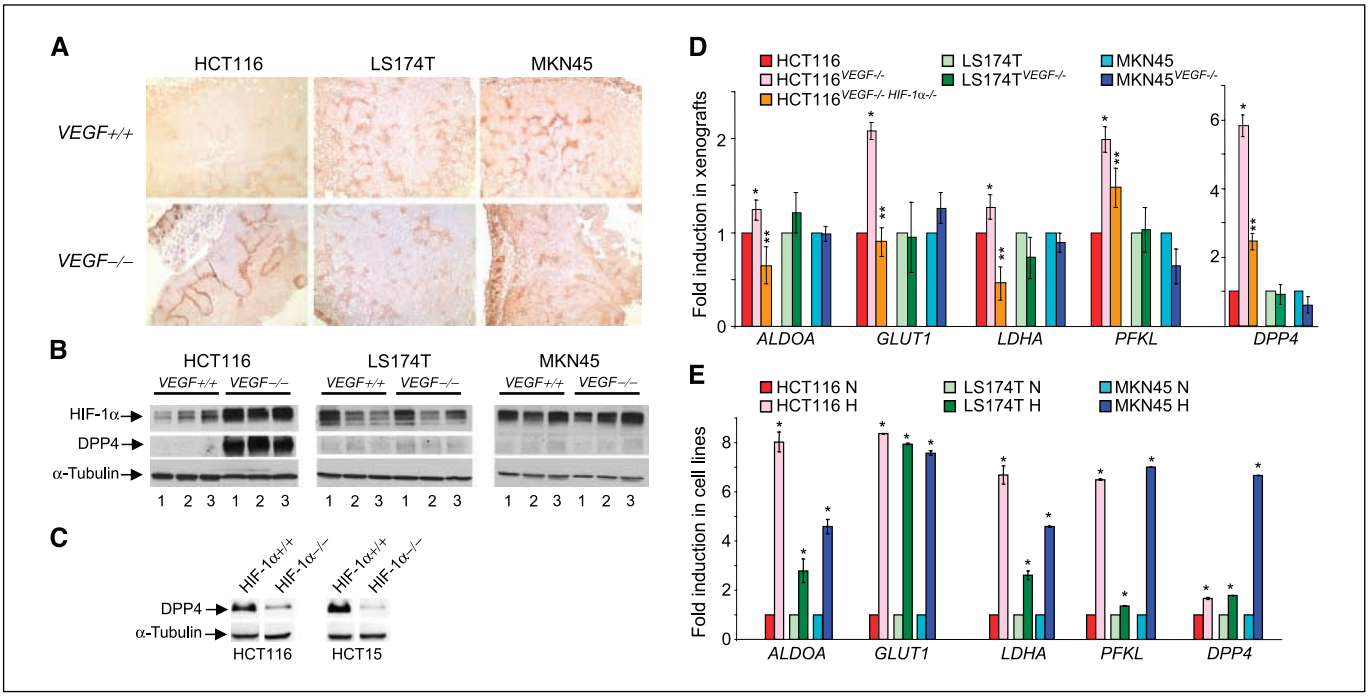

Figure 4. Analyses of intratumoral hypoxia, expression of HIF-1α and HIF-1 target genes in various xenografts and cell lines. *A,* immunohistochemistry for pimonidazole adducts, which are an indicator of hypoxia, in tumor xenografts. *B,* Western blot for HIF-1α and DPP4 expression in tumor xenografts. Three separate xenografts (*lanes 1, 2*, and *3*) at ~0.4 cm^3 in size, were harvested and subjected to Western blot for HIF-1α and DPP4. α-Tubulin was the control for loading. *C,* Western blot for DPP4 expression in *HIF-1α+/+* and *HIF-1α−/−* cell lines. *D,* fold induction of HIF-1 target genes in xenografts. *ALDOA,* aldolase A; *GLUT1,* glucose transporter 1; *LDHA,* lactate dehydrogenase A; *PFKL,* phosphofructokinase, liver; and *DPP4,* dipeptidyl peptidase IV, relative to β-actin, were measured in knockout xenografts by real-time reverse transcription-PCR. *Columns,* mean values relative to parental xenografts; *bars,* SD (n = 9). *, $P < 0.01$ comparing the *VEGF−/−* xenografts with parental *VEGF+/+* xenografts; **, $P < 0.01$ comparing *VEGF−/−HIF-1α−/−* with *VEGF−/−* xenografts. *E,* fold induction of HIF-1 target genes in cell lines grown under normoxia or hypoxia. *N,* normoxia; *H,* hypoxia. *ALDOA, GLUT1, LDHA, PFKL*, and *DPP4*, relative to β-actin, were measured in cell lines under hypoxia by real-time reverse transcription-PCR. *Columns,* mean values relative to normoxia; *bars,* SD (n = 9). *, $P < 0.01$ comparing hypoxic with normoxic conditions.

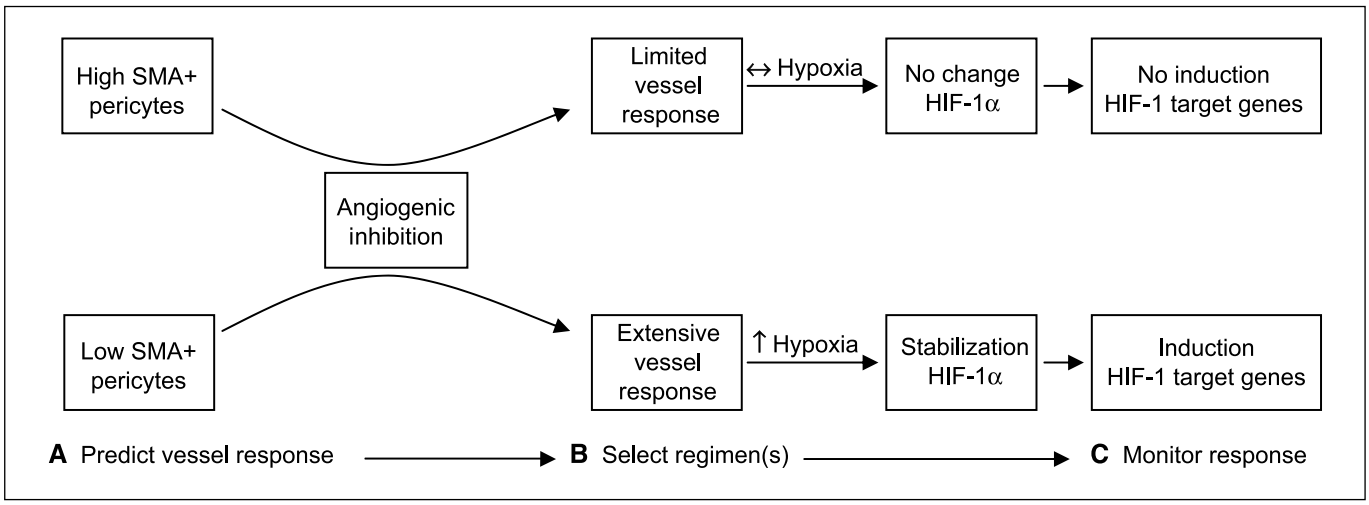

Figure 5. Diagram of potential predictors and markers of vessel response to antiangiogenic therapy. *A,* our data show that tumors with high SMA+ pericytes exhibited a limited vessel response to angiogenic inhibition (LS174T and MKN45). In contrast, tumors with low SMA+ pericytes exhibited extensive vessel response (HCT116). Thus, the extent of SMA+ staining pericytes in a tumor might correlate with the extent of vessel response to antiangiogenic therapy. *B,* the ability to predict vessel response might facilitate the selection of the most effective antiangiogenic regimen(s). *C,* our data show that tumors with limited vessel responses did not induce HIF-1 target genes. In contrast, tumors with extensive vessel responses significantly induced HIF-1 target genes. Thus, the induction of HIF-1 target genes might be a marker to monitor tumor vessel response.

To identify novel HIF-1 target genes that are induced upon VEGF inhibition, we subjected HCT116$^{VEGF-/-}$ and HCT116$^{VEGF-/-HIF-1\alpha-/-}$ xenografts to global gene expression analyses using Affymetrix U133A GeneChip. We screened for genes with at least 2-fold decreased expression in HCT116$^{VEGF-/-HIF-1\alpha-/-}$ xenografts compared with HCT116$^{VEGF-/-}$ xenografts. As HIF-1 target genes are induced by the binding of HIF-1 to hypoxia-response elements, we also screened for genes with a hypoxia-response element sequence [(A/G)CGTG] in their promoters (33).

We identified *DPP4* as the most significantly down-regulated gene by loss of HIF-1α. DPP4, also known as CD26, is a 110-kDa glycoprotein that is expressed on numerous cell types and is characterized by its dipeptidyl peptidase IV enzymatic activity (34). As such, DPP4 has multiple biological functions, including glucose homeostasis, immunoregulation, signal transduction, and apoptosis (35, 36). We were particularly intrigued by DPP4, as it has well-described roles in cancer progression (36). Furthermore, DPP4 has been shown to be easily measurable in patient serum (37). To validate the microarray results, we examined DPP4 expression in tumor xenografts. In HCT116$^{VEGF-/-}$ xenografts, there was an ~6-fold induction of *DPP4* mRNA (Fig. 4*D*) and >10-fold induction of DPP4 protein (Fig. 4*B*). Notably, *DPP4* induction in HCT116$^{VEGF-/-}$ xenografts, compared with parental HCT116 xenografts, was more than the other known HIF-1 target genes tested (Fig. 4*D*). The induction of *DPP4* was HIF-1–dependent, as there was a reversal of induction in HCT116$^{VEGF-/-HIF-1\alpha-/-}$ xenografts compared with HCT116$^{VEGF-/-}$ xenografts (Fig. 4*D*). Furthermore, disruption of *HIF-1α* in HCT116 and HCT15 cells led to an ~5-fold decreased expression of DPP4 (Fig. 4*C*). These data show that *DPP4* is a novel HIF-1 target gene. Like the known HIF-1 target genes, *DPP4* was induced in HCT116$^{VEGF-/-}$ xenografts in which VEGF inhibition induced hypoxia and stabilization of HIF-1α. In contrast, there was no induction of DPP4 in LS174T$^{VEGF-/-}$ and MKN45$^{VEGF-/-}$ xenografts in which VEGF inhibition did not induce hypoxia or stabilize HIF-1α (Fig. 4*B* and *D*). As DPP4 is secreted in the serum, its identification as a novel HIF-1 target gene introduces the possibility that it may be a marker of vessel response to antiangiogenic therapy.

To control for the possibility that the LS174T and MKN45 xenografts could not induce HIF-1 target genes at the cellular level, we examined the cell lines under *in vitro* normoxic and hypoxic culture conditions (Fig. 4*E*). When grown under hypoxic culture conditions, LS174T and MKN45 cells, like HCT116 cells, robustly induced HIF-1 target genes such as *ALDOA, GLUT1, LDHA, PFKL*, and *DPP4*. These data show that LS174T and MKN45 cells do respond to hypoxia by induction of HIF-1 target genes. Thus, the lack of induction of HIF-1 target genes, in the LS174T$^{VEGF-/-}$ and MKN45$^{VEGF-/-}$ xenografts, was likely due to a lack of significant alterations in tumor vessel perfusion and hypoxia. Altogether, these data show that the induction of HIF-1 target genes, including *DPP4,* in tumor xenografts is an indicator of HIF-1α stabilization, and thus, the extent of tumor vessel response to antiangiogenic therapy. To corroborate the above findings, we treated established HCT116, LS174T, and MKN45 xenografts with anti-VEGF antibodies. Indeed, the extent of vessel regression was associated with the induction of *DPP4* (Supplementary Fig. S1).

Discussion

Several novel conclusions and promising clinical implications could be drawn from this study. These studies show that HCT116 tumors are dependent on VEGF, whereas LS174T and MKN45 tumors are not dependent on VEGF. HCT116$^{VEGF-/-}$ xenografts were marked by inadequate residual vessels and decreased tumor perfusion. These alterations led to increased intratumoral hypoxia, stabilization of HIF-1α, and induction of HIF-1 target genes from the tumor epithelial cell compartment (Fig. 5). In contrast, LS174T$^{VEGF-/-}$ and MKN45$^{VEGF-/-}$ xenografts had grossly maintained vessels and tumor perfusion. Thus, there was neither stabilization of HIF-1α nor induction of HIF-1 target genes (Fig. 5). Currently, there are no proven biomarkers to monitor the efficacy of antiangiogenic therapy in patients. Our findings suggest that the induction of HIF-1 target genes distinguishes subsets of tumors that develop significant vessel regression and tumor response to antiangiogenic therapy. Thus, the induction, or lack of induction, of HIF-1 target genes might be used to monitor the extent of tumor

vessel response (Fig. 5*C*). One HIF-1 target gene that may be promising as a protein marker is DPP4, as it might have biological roles in cancer progression, and can be measured in the serum (36, 37).

Our data also suggest that the tumor pericyte subpopulation might be correlated with the extent of vessel response to antiangiogenic therapy. Consistent with the literature, we found that tumors with endothelial tubes well-protected by SMA-expressing pericytes, such as LS174T and MKN45, might be refractory to antiangiogenic therapy. In contrast, tumors with low recruitment of SMA-expressing pericytes, such as HCT116, have significant vessel regression in response to antiangiogenic therapy. These data also provide two novel insights into pericyte biology. We show that SMA+ pericytes are more protective than NG2+ pericytes upon VEGF withdrawal (Fig. 3). This suggests that various pericyte subpopulations might act through different mechanisms to protect endothelial tubes. Further investigations in this area might yield agents that disrupt effective pericyte signaling. These data also show that different tumor xenografts are composed of different ratios of NG2+ or SMA+ pericyte subpopulations. This suggests that there might be tumor cell–derived factor(s) that recruit the various pericyte subpopulations. Further investigation in this area might yield agents that disrupt effective pericyte recruitment.

The ability to predict or monitor the extent of tumor vessel response might guide the selection of more effective antiangiogenic regimens (Fig. 5*B*). For example, tumors that might not extensively respond to antiangiogenic therapy (i.e., LS174T and MKN45), might respond better to combination therapy with bevacizumab plus standard chemotherapy. In contrast, tumors that are predicted to develop extensive vessel regression (i.e., HCT116), might respond to monotherapy with bevacizumab or multitargeted tyrosine kinase inhibitors. Furthermore, being able to monitor tumor vessel responses, through the induction of HIF-1 target genes, would be useful for validating and/or modulating the antiangiogenic regimen.

Altogether, these data suggest potential strategies to maximize the efficacy of antiangiogenic therapy. These preclinical data should be interpreted within the context of the tumor-specific genetic alterations examined, as well as the mouse xenograft model system used. This model system allowed us to determine the effects of complete and specific ablation of VEGF on tumor vessel response; however, the clinical scenario is likely more complex due to confounding variables related to pharmacokinetics and pharmacodynamics. Certainly, further investigations are warranted and ongoing. The extent of tumor vessel response in patients receiving antiangiogenic therapy will need to be correlated with the induction of HIF-1 target genes, as well as basal tumor vasculature characteristics. The biological roles of DPP4 in the antiangiogenic response remain unclear. Whether LS174T and MKN45 xenografts use alternative angiogenic pathways remains to be determined. Nevertheless, these are the first data to show that (*a*) quantifying SMA staining pericytes might predict the extent of tumor antiangiogenic response, (*b*) HIF-1 target genes are good indicators of the extent of tumor antiangiogenic response, and (*c*) DPP4 is a novel marker of HIF-1 activity in tumors.

Acknowledgments

Received 4/30/2007; revised 11/10/2007; accepted 1/16/2008.

Grant support: NIH grant K22CA111897, The University of Michigan Comprehensive Cancer Center Pilot Project Award (NIH P30 CA46592), and the Michigan Gut Peptide Research Center Pilot Feasibility Award (NIH P30 DK34933; L.H. Dang).

The costs of publication of this article were defrayed in part by the payment of page charges. This article must therefore be hereby marked *advertisement* in accordance with 18 U.S.C. Section 1734 solely to indicate this fact.

We thank Alfred Chang and Gregory Kalemkerian for insightful suggestions on the manuscript; Joe Washburn, James MacDonald, and Kerry Innes at the University of Michigan Comprehensive Cancer Center Microarray Facility for assistance with microarray analyses; the University of Michigan Comprehensive Cancer Center tissue core facility for assistance with tumor processing; Rob Patten for helpful technical advice; and Linda Hartwig and Pam Varga for administrative assistance.

References

1. Brown LF, Berse B, Jackman RW, et al. Expression of vascular permeability factor (vascular endothelial growth factor) and its receptors in adenocarcinomas of the gastrointestinal tract. Cancer Res 1993;53:4727–35.
2. Carmeliet P, Ferreira V, Breier G, et al. Abnormal blood vessel development and lethality in embryos lacking a single VEGF allele. Nature 1996;380:435–9.
3. Ferrara N, Carver-Moore K, Chen H, et al. Heterozygous embryonic lethality induced by targeted inactivation of the VEGF gene. Nature 1996;380:439–42.
4. Hurwitz H, Fehrenbacher L, Novotny W, et al. Bevacizumab plus irinotecan, fluorouracil, and leucovorin for metastatic colorectal cancer. N Engl J Med 2004;350:2335–42.
5. Sandler A, Gray R, Perry MC, et al. Paclitaxel-carboplatin alone or with bevacizumab for non-small-cell lung cancer. N Engl J Med 2006;355:2542–50.
6. Schneider BP, Sledge GW, Jr. Drug insight: VEGF as a therapeutic target for breast cancer. Nat Clin Pract Oncol 2007;4:181–9.
7. Escudier B, Eisen T, Stadler WM, et al. Sorafenib in advanced clear-cell renal-cell carcinoma. N Engl J Med 2007;356:125–34.
8. Motzer RJ, Michaelson MD, Rosenberg J, et al. Sunitinib efficacy against advanced renal cell carcinoma. J Urol 2007;178:1883–7.
9. Goodman VL, Rock EP, Dagher R, et al. Approval summary: sunitinib for the treatment of imatinib refractory or intolerant gastrointestinal stromal tumors and advanced renal cell carcinoma. Clin Cancer Res 2007;13:1367–73.
10. Jain RK, Duda DG, Clark JW, Loeffler JS. Lessons from phase III clinical trials on anti-VEGF therapy for cancer. Nat Clin Pract Oncol 2006;3:24–40.
11. Harris AL. Hypoxia—a key regulatory factor in tumour growth. Nat Rev Cancer 2002;2:38–47.
12. Koukourakis MI, Giatromanolaki A, Sivridis E, et al. Lactate dehydrogenase-5 (LDH-5) overexpression in non-small-cell lung cancer tissues is linked to tumour hypoxia, angiogenic factor production and poor prognosis. Br J Cancer 2003;89:877–85.
13. Koukourakis MI, Bentzen SM, Giatromanolaki A, et al. Endogenous markers of two separate hypoxia response pathways (hypoxia inducible factor 2α and carbonic anhydrase 9) are associated with radiotherapy failure in head and neck cancer patients recruited in the CHART randomized trial. J Clin Oncol 2006;24:727–35.
14. Blagosklonny MV. Hypoxia-inducible factor: Achilles' heel of antiangiogenic cancer therapy [review]. Int J Oncol 2001;19:257–62.
15. Franco M, Man S, Chen L, et al. Targeted anti-vascular endothelial growth factor receptor-2 therapy leads to short-term and long-term impairment of vascular function and increase in tumor hypoxia. Cancer Res 2006;66:3639–48.
16. Dang DT, Chen F, Gardner LB, et al. Hypoxia-inducible factor-1α promotes nonhypoxia-mediated proliferation in colon cancer cells and xenografts. Cancer Res 2006;66:1684–936.
17. Kohli M, Rago C, Lengauer C, Kinzler KW, Vogelstein B. Facile methods for generating human somatic cell gene knockouts using recombinant adeno-associated viruses. Nucleic Acids Res 2004;32:3–10.
18. Rofstad EK, Maseide K. Radiobiological and immunohistochemical assessment of hypoxia in human melanoma xenografts: acute and chronic hypoxia in individual tumours. Int J Radiat Biol 1999;75:1377–93.
19. Pfaffl MW. A new mathematical model for relative quantification in real-time RT-PCR. Nucleic Acids Res 2001;29:2003–7.
20. Armulik A, Abramsson A, Betsholtz C. Endothelial/pericyte interactions. Circ Res 2005;97:512–23.
21. Darland DC, Massingham LJ, Smith SR, et al. Pericyte production of cell-associated VEGF is differentiation-dependent and is associated with endothelial survival. Dev Biol 2003;264:275–88.
22. Suri C, Jones PF, Patan S, et al. Requisite role of angiopoietin-1, a ligand for the TIE2 receptor, during embryonic angiogenesis. Cell 1996;87:1171–80.
23. Sato TN, Tozawa Y, Deutsch U, et al. Distinct roles of the receptor tyrosine kinases Tie-1 and Tie-2 in blood vessel formation. Nature 1995;376:70–4.
24. Lindahl P, Johansson BR, Leveen P, Betsholtz C. Pericyte loss and microaneurysm formation in PDGF-B-deficient mice. Science 1997;277:242–5.
25. Benjamin LE, Golijanin D, Itin A, Pode D, Keshet E. Selective ablation of immature blood vessels in established human tumors follows vascular endothelial growth factor withdrawal. J Clin Invest 1999;103:159–65.
26. Gee MS, Procopio WN, Makonnen S, et al. Tumor vessel development and maturation impose limits on the effectiveness of anti-vascular therapy. Am J Pathol 2003;162:183–93.

27. Bergers G, Song S, Meyer-Morse N, Bergsland E, Hanahan D. Benefits of targeting both pericytes and endothelial cells in the tumor vasculature with kinase inhibitors. J Clin Invest 2003;111:1287–95.

28. Abramsson A, Lindblom P, Betsholtz C. Endothelial and nonendothelial sources of PDGF-B regulate pericyte recruitment and influence vascular pattern formation in tumors. J Clin Invest 2003;112:1142–51.

29. Schlingemann RO, Rietveld FJ, Kwaspen F, et al. Differential expression of markers for endothelial cells, pericytes, and basal lamina in the microvasculature of tumors and granulation tissue. Am J Pathol 1991;138:1335–47.

30. Semenza GL. HIF-1 and tumor progression: pathophysiology and therapeutics. Trends Mol Med 2002;8:S62–7.

31. Semenza GL. Targeting HIF-1 for cancer therapy. Nat Rev Cancer 2003;3:721–32.

32. Giaccia A, Siim BG, Johnson RS. HIF-1 as a target for drug development. Nat Rev Drug Discov 2003;2:803–11.

33. Okino ST, Chichester CH, Whitlock JP, Jr. Hypoxia-inducible mammalian gene expression analyzed *in vivo* at a TATA-driven promoter and at an initiator-driven promoter. J Biol Chem 1998;273:23837–43.

34. Darmoul D, Lacasa M, Chantret I, Swallow DM, Trugnan G. Isolation of a cDNA probe for the human intestinal dipeptidylpeptidase IV and assignment of the gene locus DPP4 to chromosome 2. Ann Hum Genet 1990;54:191–7.

35. Marguet D, Baggio L, Kobayashi T, et al. Enhanced insulin secretion and improved glucose tolerance in mice lacking CD26. Proc Natl Acad Sci U S A 2000;97:6874–9.

36. Pro B, Dang NH. CD26/dipeptidyl peptidase IV and its role in cancer. Histol Histopathol 2004;19:1345–51.

37. de la Haba-Rodriguez J, Macho A, Calzado MA, et al. Soluble dipeptidyl peptidase IV (CD-26) in serum of patients with colorectal carcinoma. Neoplasma 2002;49:307–11.

Hypoxia-Inducible Factor-1 Target Genes as Indicators of Tumor Vessel Response to Vascular Endothelial Growth Factor Inhibition

Duyen T. Dang, Sang Y. Chun, Kyunghee Burkitt, et al.

Cancer Res 2008;68:1872-1880.